PHYSICS

Shaping nanoparticle fingerprints at the interface of cholesteric droplets

Lisa Tran[1]*†, Hye-Na Kim[2], Ningwei Li[3], Shu Yang[2], Kathleen J. Stebe[4], Randall D. Kamien[1], Martin F. Haase[5]*

The ordering of nanoparticles into predetermined configurations is of importance to the design of advanced technologies. Here, we balance the interfacial energy of nanoparticles against the elastic energy of cholesteric liquid crystals to dynamically shape nanoparticle assemblies at a fluid interface. By adjusting the concentration of surfactant that plays the dual role of tuning the degree of nanoparticle hydrophobicity and altering the molecular anchoring of liquid crystals, we pattern nanoparticles at the interface of cholesteric liquid crystal emulsions. In this system, interfacial assembly is tempered by elastic patterns that arise from the geometric frustration of confined cholesterics. Patterns are tunable by varying both surfactant and chiral dopant concentrations. Adjusting the particle hydrophobicity more finely by regulating the surfactant concentration and solution pH further modifies the rigidity of assemblies, giving rise to surprising assembly dynamics dictated by the underlying elasticity of the cholesteric. Because particle assembly occurs at the interface with the desired structures exposed to the surrounding water solution, we demonstrate that particles can be readily cross-linked and manipulated, forming structures that retain their shape under external perturbations. This study serves as a foundation for better understanding inter-nanoparticle interactions at interfaces by tempering their assembly with elasticity and for creating materials with chemical heterogeneity and linear, periodic structures, essential for optical and energy applications.

INTRODUCTION

The ability to organize nanoparticles into designed arrangements is of interest for a wide range of material applications, including nanomedicine, energy harvesting, catalysis, and optical devices (*1*, *2*). Recently, structured assemblies of nanoparticles have been achieved within the bulk of polymer matrices (*3*), block copolymers (*4*), and liquid crystals (*5*–*10*). However, traditional polymers and block copolymers are not easily reconfigurable with external stimuli, limiting their use in applications that require dynamic responses. Furthermore, although we have demonstrated that liquid crystals do reconfigure with changes in temperature and surfactant concentration (*11*), the assemblies achieved within liquid crystals thus far have nanoparticles dispersed and embedded within the bulk. This limits chemical access to the resultant nanoassemblies, which is essential for their production and use in sensing and optical applications (*2*, *12*–*16*).

Our previous work has shown that cholesteric liquid crystals can alter their arrangements with changing boundary curvature, developing a fingerprint texture that often has twisted, double-spiraled, focal conic domains, which is composed of alternating regions of liquid crystal anchoring to a surface (*11*). Furthermore, for a cholesteric to produce focal conic domains, it must deform its interface into a hilly topography, with each hill accommodating a double spiral, generating nontrivial interfacial curvature (*11*, *17*–*19*). These phenomena establish an interplay between bulk elasticity and surface tension. It remains unexplored how this interplay shapes nanoparticle assemblies, as nanoparticles can kinetically arrest and aggregate, unlike molecular surfactants, introducing rigidity to the interface. Can surface-active nanoparticles follow liquid crystal patterning? What is the role of nanoparticle surface chemistry in the response of assemblies to the elasticity of liquid crystals?

Here, we demonstrate the structuring of surfactants and nanomaterials at the interface of cholesteric liquid crystal droplets in aqueous solutions. We realize interfacial nanoparticle assemblies that are shaped by the elastic field of liquid crystals, a phenomenon previously predicted by simulations (*20*, *21*) but is now accomplished experimentally. With the use of surfactant-modified nanoparticles that attach to the water-liquid crystal interface, we create patterned nanoparticle-decorated emulsions at high densities and with cross-linkable, assembled arrangements that are dynamically controllable through the underlying elastic field. This approach is fundamentally different from both the assembly of nanomaterials within liquid crystal defects and the assembly of microparticles at liquid crystal interfaces (*22*–*25*), as it does not rely on bulk defects but instead on surface anchoring—the molecular orientation of liquid crystals at the confining boundaries. This method further exploits the intrinsic ability of cholesteric liquid crystals to form complex but ordered surface patterns. Moreover, our findings elucidate a previously unexplored regime in particle-stabilized emulsion systems: The interfacial adsorption energy of the nanoparticles that we use is such that their aggregation is moderated by the liquid crystal elastic energy, revealing that their adsorption behavior follows kinetics reminiscent of nucleation and growth.

RESULTS AND DISCUSSION

Patterned segregation of lipids and particles at the cholesteric-water interface

A homogeneous mixture of 5CB (4-cyano-4′-pentylbiphenyl) doped with CB15 [(*S*)-4-cyano-4-(2-methylbutyl)biphenyl] is emulsified to

[1]Department of Physics and Astronomy, University of Pennsylvania, 209 South 33rd Street, Philadelphia, PA 19104, USA. [2]Department of Materials Science and Engineering, University of Pennsylvania, 3231 Walnut Street, Philadelphia, PA 19104, USA. [3]Department of Mechanical and Industrial Engineering, University of Massachusetts Amherst, 160 Governors Drive, Amherst, MA 01003, USA. [4]Department of Chemical and Biomolecular Engineering, University of Pennsylvania, 220 South 33rd Street, Philadelphia, PA 19104, USA. [5]Department of Chemical Engineering, Rowan University, 600 North Campus Drive, Glassboro, NJ 08028, USA.
*Corresponding author. Email: ltran@sas.upenn.edu (L.T.); haasem@rowan.edu (M.F.H.)
†Present address: Department of Chemical Engineering, Columbia University, 500 West 120th Street, New York, NY 10027, USA.

form polydisperse droplets in an aqueous phase, stabilized by surfactants that induce homeotropic anchoring. We analyze droplets that range from ~50 to ~500 μm in diameter. Homeotropic anchoring is achieved using hydrocarbon surfactants with hydrophilic heads and hydrophobic tails. The hydrophobic tails intercalate between liquid crystal molecules, causing them to align parallel to the tail, perpendicular to the interface (Fig. 1A) (*11*, *14*, *26*). A cholesteric breaks both orientational and translational symmetries, as its molecules have an energetic tendency not only to align with one another but also to have a bulk twist, stacking molecules in a helical fashion and imparting a periodic phase into the material. When a cholesteric is bounded by a surface that induces homeotropic anchoring, there is no way for the twisting molecules to orient near the boundary without frustrating either the anchoring energy or the twist energy. At moderate homeotropic anchoring strengths, alternating regions of homeotropic and planar anchoring occur at the surface because of periodic violation of the homeotropic boundary condition by the twist elastic energy, as depicted in Fig. 1A (*11*). Stripes of planar anchoring are created at the surface by the cholesteric twist. We used the competition between the cholesteric's energetic preference to twist and a homeotropic boundary condition that aligns molecules perpendicular to the boundary to generate surface stripes.

From the use of the fluorescently labeled lipid TR-DLPC (Materials and methods), we find that not only do lipids induce homeotropic anchoring of the cholesteric but also the cholesteric subsequently segregates the lipids at the interface, excluding them from twist regions incompatible with the anchoring (Fig. 1B). This generates a system with an inhomogeneous, dynamic boundary condition. At 0.005 mM TR-DLPC, thin stripes form double-spiraled focal conic domains, visible under confocal microscopy from the creation of lipid-depleted stripes along twist regions. As the TR-DLPC concentration is increased to 0.01 mM, more lipids adsorb to the interface. The thickness of the lipid-filled stripes increases, disrupting the stripe pattern as the twist energy is further frustrated by the increasing homeotropic anchoring energy. The surface pattern disappears entirely when the interface is fully saturated with lipids—the homeotropic anchoring is so strong that it prevents the cholesteric from twisting at the surface.

Can the same mechanism of lipid patterning be used to pattern nanoparticles? To explore this question, we functionalize nanoparticles with surfactants (Fig. 1C), according to the literature (*27*–*29*). To this end, ionic surfactants are selected to electrostatically adsorb to the surfaces of positively or negatively charged particles, respectively. This in situ modification of altering nanoparticle hydrophobicity facilitates the use of surfactants that have been proven to change liquid crystal anchoring at the liquid crystal–water interface (*26*). The surfactants used in these experiments, either anionic sodium alkyl sulfate (SA_nS) or cationic trimethyl alkylammonium bromide (A_nTAB), where n indicates the alkyl chain length, have each been shown to induce homeotropic anchoring for 5CB (*11*, *26*). Moreover, this method of surface modification provides flexibility in material composition of the nanoparticles. Two types of fluorescent nanoparticles are used to study the effect of nanoparticle size and surface chemistry: positively charged, amine-functionalized, 200-nm particles and negatively charged, bare, 30-nm silica nanoparticles. The former are in situ surface modified with SA_nS, and the latter with A_nTAB. Similar to the lipids in Fig. 1B, nanoparticles are able to segregate into stripes that have homeotropic anchoring, but only under specific solution conditions, as depicted in Fig. 1C and as demonstrated in the confocal micrographs of Fig. 1D. Nanoparticle concentration, surfactant concentration, nanoparticle size, surfactant tail length, and solution pH are all found to influence the behavior of nanoparticles at the cholesteric-water interface.

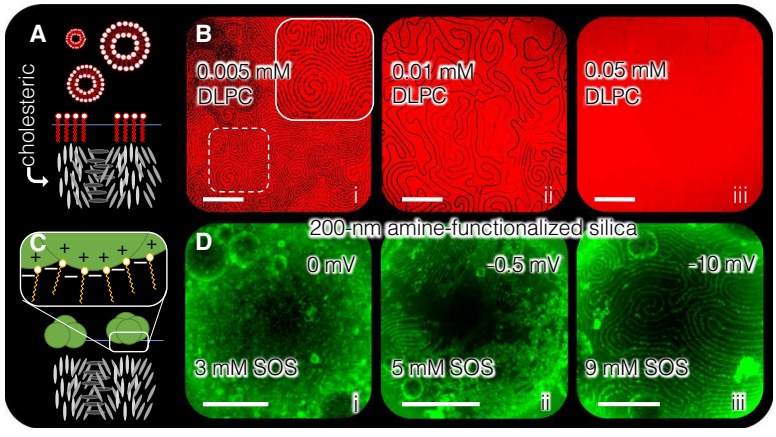

Fig. 1. Lipid and nanoparticle segregation at the cholesteric liquid crystal–water interface. (**A**) Cholesterics (gray) must twist along the surface to have as much homeotropic anchoring as possible from the presence of lipids in the surrounding water phase. The hydrophobic tails of the lipids prefer the liquid crystal phase, causing liquid crystal molecules to lie parallel to the tail and thus perpendicular to the interface. Twist regions with molecules tangent to the interface exclude traditional, molecular surfactants, such as lipids (red). (**B**) Laser scanning confocal microscopy data of lipids (TR-DLPC, red) at the cholesteric-water interface demonstrate segregation of the lipids into stripes that follow the underlying cholesteric order. As lipid concentration increases (i to iii), surface stripes become wider and more disordered (ii) until twist regions are forced away from the surface as a result of the lipids saturating the interface (iii). (**C**) Surfactant-decorated nanoparticles, made surface active from the electrostatic grafting of molecular surfactants to the nanoparticle surface, are also found to align with molecules perpendicular to the interface, forming patterned assemblies. (**D**) Projections of laser scanning confocal microscopy *z* stacks of nanoparticles (green) on cholesteric droplets demonstrate how nanoparticles surface modified by surfactants can follow the underlying cholesteric patterning at the cholesteric-water interface. Electrostatic surface functionalization allows flexible surface chemistry. The data show that amine-functionalized silica nanoparticles, which have positive surface charge, now become surface active after modification by negatively charged surfactant, SOS. Increasing the SOS concentration to obtain nanoparticles with sufficiently negative zeta potentials is needed for the particles to segregate into stripes (iii). Numbers on the upper right corners of micrographs are system zeta potential measurements. Scale bars, 50 μm.

The degree of surfactant coverage on nanoparticles determines the particle segregation behavior on cholesteric droplets. Confocal micrographs depicting the behavior of 200-nm, fluorescent, silica nanoparticles on cholesteric droplets are given in Fig. 1D and fig. S1. The droplets are emulsified by hand shaking in a nanoparticle dispersion of 10^{-3} weight % (wt %) with varying sodium octyl sulfate (SOS) concentrations. The degree of surfactant coverage on the nanoparticles is determined by zeta potential measurements of selected samples (Fig. 1D and fig. S2B) (*30*). The amine-functionalized particles alone have a zeta potential of 36 mV, confirming a highly positive surface charge that provides enough electrostatic repulsion for colloidal stability—that is, the nanoparticles are well dispersed and hydrophilic. A solution of these nanoparticles with 3 mM SOS results in a zeta potential of 0 mV, indicating saturated monolayer adsorption of SOS on the particles. At these low SOS concentrations (8 mM and less), the nanoparticles become hydrophobic and strongly aggregate at the cholesteric interface and in the solution (Fig. 1D, i and ii). Increasing the SOS concentration results in charge reversal with further decrease of the zeta potential. This indicates the onset of SOS double-layer formation on the particles with increasing SOS concentration, with negatively charged sulfate groups oriented toward the aqueous solution. It is only around and slightly above 10 mM that the nanoparticles are better dispersed and well ordered within the homeotropic stripes of the cholesteric droplet (Fig. 1D, iii, and fig. S1, green). The degree of hydrophobicity of the nanoparticles must decrease for them to aggregate less, with their mutual repulsion facilitated by the slight surfactant double layer. However, decreasing the nanoparticle hydrophobicity further by increasing the SOS concentration to 25 mM results in fewer nanoparticles at the droplet interface, suggesting that the double layer has progressed such that the nanoparticle surface charge is dominated by hydrophilic head groups, causing the nanoparticles themselves to become hydrophilic again. The surfactant concentration must be moderated to enable both particle dispersion and particle adsorption onto the liquid crystal–water interface.

Effect of particle hydrophobicity, particle size, and pH of solution

For the uniform segregation of surfactant-modified nanoparticles into homeotropic stripes, we identify three additional criteria.

1) Because the degree of hydrophobicity is key to nanoparticle dispersion and wetting behavior, it follows that the length of the surfactant tail also affects the nanoparticle behavior, as shown in fig. S2 (*31*). Shorter surfactant tail lengths offer greater colloidal stability, enabling nanoparticles to be dispersed enough for them to adsorb to the cholesteric interface with minimal aggregation. This, in turn, enables particles to better follow homeotropic stripes and to fully deplete from planar, twist regions. Because of this, we mainly use surfactants with a tail length of eight carbons for nanoparticle surface modification.

2) The nanoparticle size also affects their aggregation behavior. At a fixed surfactant and nanoparticle concentration, the 200-nm particle system has a greater degree of particle aggregation compared to those with 30-nm particles. Working with smaller nanoparticles is thus more advantageous as the particle aggregation is better managed by larger particle surface areas and greater thermal activity. To this end, we use bare, untreated, 30-nm silica particles with trimethyloctylammonium bromide (C_8TAB).

3) The solution pH further influences nanoparticle behavior, as it affects the amount of surfactants adsorbed onto the nanoparticle surface (*30*, *32*). Zeta potential measurements with varying pH in the presence of either C_8TAB for bare silica particles or SOS for amine-functionalized particles are given in fig. S3.

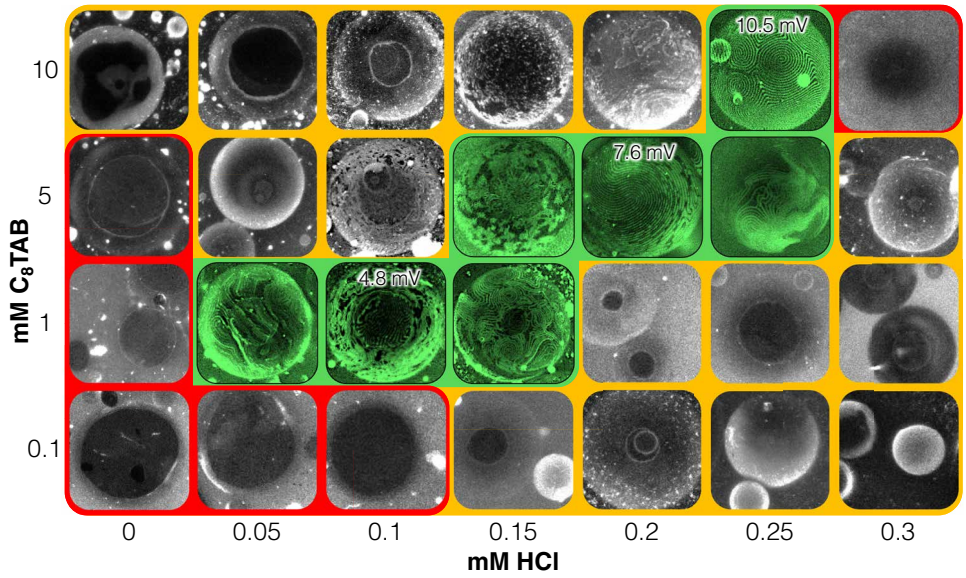

Fig. 2. State diagram for nanoparticle stripe segregation with varying concentrations of HCl and C_8TAB. Segregation of surface-modified nanoparticles at the cholesteric-water interface takes place in a narrow pH and surfactant concentration range. Silica nanoparticles (30 nm) are in situ, surface functionalized with C_8TAB. Droplets of the cholesteric 5CB with 3 wt % CB15 are formed by simple vial shaking. Varying the concentration of C_8TAB and HCl shows three regions: Red regions indicate that particles do not attach to the cholesteric interface. Yellow regions signify unordered, interfacial assembly of nanoparticles. Green regions denote conditions where particles are surface active and have cholesteric ordering, forming stripes. Zeta potentials for selected systems are given at the top of micrographs. The bare silica nanoparticles have a slightly positive zeta potential that becomes more positive with increasing C_8TAB concentration, implying the presence of a slight C_8TAB double layer at their surfaces that further develops with increasing concentration. Exact acid concentrations may vary depending on the age of solutions, as systems are pH sensitive and become more acidic with time due to the absorption of carbon dioxide. Scale bars, 50 μm.

Considering the above criteria, we explore the interfacial behavior for 30-nm, bare silica nanoparticles with varying C_8TAB and hydrochloric acid (HCl) concentrations in Fig. 2. In this state diagram, red indicates no interfacial wetting of the nanoparticles, yellow indicates interfacial attachment but with aggregation, and green indicates interfacial attachment with particle segregation into cholesteric patterns.

Similar to the 200-nm, amine-functionalized system in Fig. 1D, segregation of nanoparticles into stripes occurs only within a narrow regime, where the hydrophobicity of the particles is not only not so great that the particles aggregate with one another but also not so small that they do not adsorb. At low surfactant concentrations (from 0.1 to 1 mM C_8TAB), the more basic the solution is, the more negatively charged silanol groups there are on the nanoparticle surface. At these conditions, no significant particle deposition on the droplets can be observed (red region). The resulting droplets wet the surface of the microscope slide, creating black regions in the middle of droplets in confocal micrographs. Decreasing the pH by adding HCl increases the nanoparticle hydrophobicity, bringing the system from nonattachment (red) to stripe segregation (green) to randomly organized nanoparticle aggregates (yellow), suggesting increasing hydrophobicity with decreasing pH. However, at a high surfactant concentration (from 5 to 10 mM C_8TAB), the system starts off already hydrophobic at high pH (yellow) and crosses over to stripe segregation (green) and then nonattachment (red) with additions of HCl. This pattern is consistent with the hypothesis that, at high surfactant concentration, a slight surfactant double layer is needed at the particle surface for successful segregation within stripes. Again, too complete of a surfactant double layer will make the particles too hydrophilic, resulting in no aggregation and no interfacial attachment, as seen with 10 mM C_8TAB and 0.3 mM HCl (red).

By moderating C_8TAB and HCl concentrations to adjust particle hydrophobicity, nanoparticles can follow the cholesteric pattern, with the best particle ordering seen at 10 mM C_8TAB and 0.25 mM HCl. The increasing zeta potential of green regions with increasing C_8TAB concentration provides further evidence for the presence of a surfactant double layer on the nanoparticle surface. Before nanoparticle attachment, stripes are evident on droplets under the surfactant and acid conditions of all systems within green regions of the state diagram. Thus, before particle adsorption to the interface, in addition to modifying particle surfaces, surfactants also alter the cholesteric anchoring, likely locating in homeotropic regions (*26*). The red and yellow regions of the state diagram in Fig. 2 show the expected behavior of nanoparticles that are in situ surface-modified by surfactants, reminiscent of typical Pickering emulsions (*27*, *28*). However, the green region of the state diagram presents nontrivial behavior of nanoparticle assemblies that are influenced by the liquid crystal elasticity. The stripes formed from 1 to 5 mM C_8TAB with HCl concentrations ranging from 0 to 0.2 mM have nanoparticle stripes that do not perfectly follow the cholesteric ordering. Instead, the assemblies appear rigid and have regions with aggregated particles. Only for 5 and 10 mM C_8TAB, with 0.25 mM HCl, do the nanoparticle assemblies strongly follow the cholesteric ordering, matching the lipid results of Fig. 1B.

Controlling the width of nanoparticle-decorated stripes of flexible assemblies

To better understand the nanoparticle behavior at the condition that exhibits strong ordering by the cholesteric (0.25 mM HCl and ~10 mM C_8TAB), we adjust the nanoparticle stripe width by slightly varying the amount of C_8TAB at fixed dopant concentration (Fig. 3, A and D). Similar to the lipids system in Fig. 1B, increasing the C_8TAB concentration from 10 to 15 mM in the solution can increase the stripe thickness, but the stripes also become more disordered as the homeotropic anchoring energy increases and distorts the cholesteric twist, producing disordered stripe patterns (Fig. 3A, bottom).

The nanoparticle assemblies appear to conform to and are unfrustrated by the underlying cholesteric patterning. The particles map out the interfacial regions with homeotropic anchoring well, behaving as the lipids do in the experiment shown in Fig. 1B. Because the lipids remain mobile at the interface for that experiment, as was reported previously by Brake *et al.* (*14*), the similar behavior between the lipid and nanoparticle systems suggests that, at these conditions, the nanoparticles may also be mobile on the interface. Fluid interfacial behavior of nanoparticles has been reported previously for gold nanoparticles capped with (1-mercaptoundec-11-yl) tetra(ethylene glycol) (*33*) and for silica nanoparticles functionalized with A_nTAB with varying surfactant and salt concentrations (*34*, *35*). Our solution conditions have fine-tuned the nanoparticle hydrophobicity by adjusting surfactant concentration and pH such that the particles have both interfacial activity and colloidal stability, possibly facilitating their mobility at the cholesteric interface.

Maintaining 10 mM C_8TAB and 0.25 mM HCl, the nanoparticle stripe width can also be adjusted by tuning the pitch of the cholesteric twist. This can be accomplished by modifying the chiral dopant (CB15) concentration within 5CB, as demonstrated in the confocal micrographs in Fig. 3 (B and C). All measurements discussed thus far have been performed with 3 wt % CB15, giving a cholesteric pitch of ~5 μm, measured with the Grandjean-Cano wedge cell (*36*, *37*). Surface stripe widths are equal to half of the cholesteric pitch with unfrustrated twisting at the boundary, giving stripe widths of ~2.5 μm for 3% CB15 (*11*). Increasing the dopant concentration to 7% decreases the size of the pitch to slightly above 1 μm, giving a stripe width of around 600 nm (Fig. 3C). However, increasing the chiral dopant concentration further to 10%, with a cholesteric pitch of ~600 nm and an expected surface stripe width of ~300 nm, results in no stripes visible under the confocal microscope (Fig. 3B, bottom right). Instead, the cholesteric ordering appears as circular domains that map out the locations of cholesteric double spirals. It is intriguing that the fluorescent intensity is lower in the regions between circular domains, indicating fewer nanoparticles located at these areas, as seen also for 7% CB15 in between double spirals (Fig. 3B, ii). It is also possible that the confocal resolution is not high enough to resolve the stripe width for the 10% CB15 system. It would be interesting to view the surface of these droplets with atomic force microscope or scanning electron microscope, but polymerizing or otherwise solidifying the liquid crystal would be necessary to perform these measurements (*16*). More detailed studies are necessary. Our method of templating nanoparticle interfacial assemblies with liquid crystals still provides a plausible method to create periodic nanoparticle structures on the range of hundred of nanometers, a length scale that is often difficult to obtain with other techniques.

Nanoparticle adsorption dynamics of rigid assemblies

Visualizing the dynamics of nanoparticle deposition on liquid crystal droplets provides further insights into their interfacial behavior. Decreasing the HCl concentration slightly, from 0.25 to 0.23 mM, while maintaining particle and C_8TAB concentrations of 0.01 wt % and 10 mM, respectively, triggers the nanoparticles to slowly aggregate

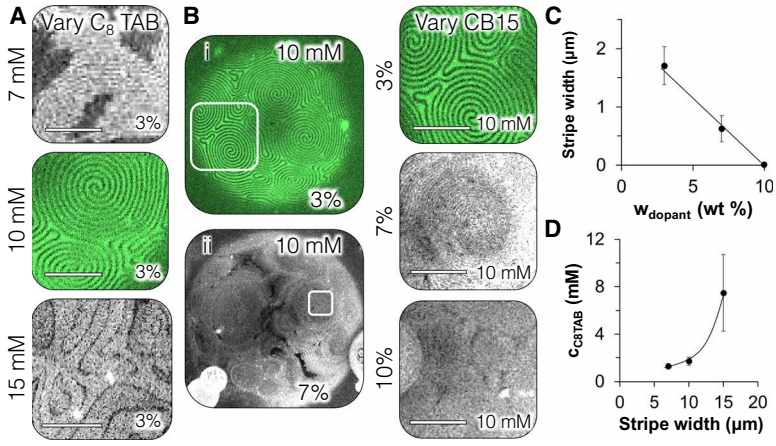

Fig. 3. Controlling the thickness of nanoparticle-filled stripes with CB15 or C_8TAB concentrations. (**A** and **D**) Similar to the lipid results in Fig.1B, the nanoparticle-filled stripe width can also be controlled with the C_8TAB concentration. (**B** and **C**) The stripe width can be tuned by adjusting the concentration of the chiral dopant CB15. By increasing the chiral dopant from 3 to 7 wt % at a fixed concentration of 10 mM C_8TAB, the stripe width decreases from ~1.7 μm to ~600 nm, corresponding to a decrease in the cholesteric pitch (A). Increasing the dopant concentration to 10 wt %, the cholesteric pitch decreases, with a projected surface stripe width on the order of ~100 nm. However, no stripe segregation at the cholesteric-water interface is evident from confocal data. Instead, nanoparticles organize into circular domains dictated by cholesteric double-spiral domains (B, bottom right). Lines in (C) and (D) are drawn to guide the eye. Scale bars, 25 μm.

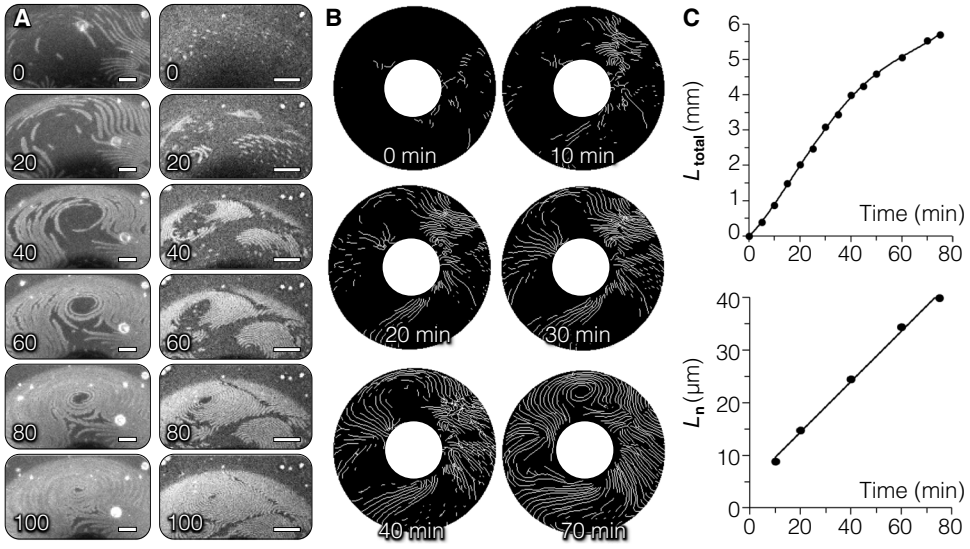

Fig. 4. Time evolution of hydrophobic nanoparticles coating a cholesteric droplet. Confocal data of nanoparticles coating two droplets with differing stripe widths are shown in (**A**), where the left column is a zoom in of the top of the droplet in (**B**). Scale bars, 25 μm. Preassembled nanoparticle clusters translate and coalesce along stripes that result from the cholesteric ordering of the droplet. The total stripe length growth rate is highest at the beginning of the interfacial attachment process and decreases with time due to the saturation of the surface with nanoparticle-filled stripes. The total stripe length of all nanoparticle stripes on the droplet shown in the left of (A) and in (B) is plotted against time in (**C**), where the total length is given by $L_{total} = \Sigma N_i \cdot L_i$, where N_i is the number of stripes with the length L_i. The total stripe length normalized by the number of stripes N_i with the length L_i is given by $L_n = (\Sigma N_i \cdot L_i)/\Sigma N_i$, which, when plotted against time, is shown in (**D**) to have a linear growth. Lines in (C) are drawn to guide the eye. Similar dynamics are seen in droplets coated with thinner nanoparticle stripes, shown in the right column of (A). A video of this process is in the supplementary materials.

with one another, becoming rigid and forming a crust at the interface after 2 hours. The process leading to crust formation around the cholesteric droplet yields surprising dynamical behaviors, as shown in Fig. 4.

The evolution of stripe lengths in Fig. 4A is measured in Fig. 4B and fig. S4A. The number of stripes, N_i, of the length, L_i, is plotted for each frame of the image sequence in fig. S4B. At the beginning of the process, there are a large number of short nanoparticle rafts that act as seeds for stripe growth, visible in frames 0 to 20 in Fig. 4A. These rafts then slide along stripes until they snap together, growing the stripes rapidly in the longitudinal stripe direction, with a slower lateral growth rate (Fig. 4A, frames 20 to 100). As the nanoparticle coverage of the droplet progresses, the number of stripe seeds decreases (fig. S4B, left), as the existing stripes continue to grow in length. The total length of the stripes ($L_{total} = \Sigma N_i \cdot L_i$) grows with time and only begins to plateau when limited by the surface area of

the droplet (Fig. 4C, top). The number-averaged length of the stripes also shows a positive, linear trend with time, further indicating that growth sites form in open space and elongate as more nanoparticles adsorb to the interface (Fig. 4C, bottom) (*38*). The homeotropic stripes are filled in first, after which the stripes continue to expand as the nanoparticles aggregate further to fully cover the cholesteric droplet.

The role of the cholesteric in structuring nanoparticle assemblies should not greatly affect the dynamics of nanoparticle interfacial attachment, as the general kinetics are likely dictated by the nanoparticles' mutual van der Waals attraction, electrostatic repulsion, and their interfacial attachment energy. Interfacial coverage of an isotropic oil droplet could also exhibit these nucleation- and growth-like behaviors. However, the elastic instabilities seen in particle film growth on curved surfaces would be greatly affected, as the cholesteric shapes the nanoparticle assemblies to be within stripes, making the growth of particle assemblies one-dimensional (1D) instead of the typical 2D surface growth (*38*). Investigating how the behavior of assembly growth on a surface is affected when the growth is predominantly 1D would be a compelling future investigation. Past studies of particle assembly growth on surfaces have been done with particles on the many-micrometer scale but not with nanoparticles (*39*–*41*). For these future studies, the cholesteric patterning could reflect the particles' mutual interaction—that is, whether the particles form structures that are more fluid or more rigid—facilitating the observation of particle deposition and growth on the nanoscale.

Cross-linking nanoparticles into cholesteric textures

Cholesteric liquid crystal surface patterns can also serve as templates for nanoparticle assemblies. Because the assemblies are guaranteed to be at droplet surfaces and are in contact with the water phase, they are physically cross-linkable by simple chemical additions to the surrounding solution. After aligning nanoparticle assemblies at 5 mM C_8TAB and 0.2 mM HCl, we introduce 0.5 mM lanthanum chloride ($LaCl_3$) to the solution. $LaCl_3$ strongly decreases the electrostatic repulsion between particles and specifically adsorbs onto the silica surface, likely facilitating electrostatic bridging, resulting in silica nanoparticles strongly binding to one another (*42*).

The integrity of the cross-linked nanoparticle assemblies is tested by heating and cooling the cholesteric droplet to and from the isotropic phase (Fig. 5). This quenches the cholesteric, disrupting the bulk ordering and disturbing the surface pattern formed by the cholesteric. Comparison of a cholesteric droplet before (Fig. 5A) and after (Fig. 5B) this quenching shows that the cholesteric pattern has been thrown into disarray. However, the nanoparticle assemblies retain their linear structure, demonstrating that the cholesteric can successfully template nanoparticles into cross-linkable wires. Without cross-linking by $LaCl_3$, the nanoparticle assemblies generally do not preserve their linear structure after the cholesteric droplets are quenched (fig. S5).

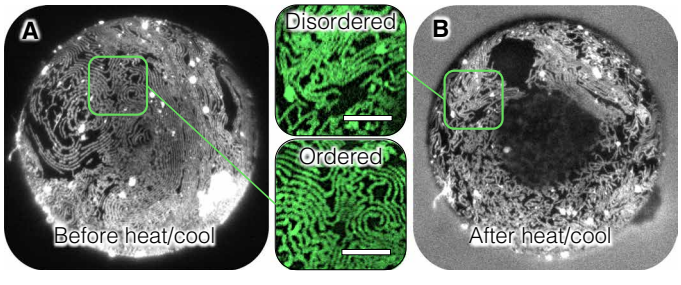

Fig. 5. Cross-linking nanoparticle assemblies and destroying cholesteric ordering with temperature. (**A**) A confocal micrograph shows the cross-linked nanoparticles on a cholesteric droplet. The integrity of the cross-linked nanoparticle stripes is tested by rapidly heating the droplet to and cooling from the isotropic phase to disrupt the cholesteric ordering. (**B**) The confocal micrograph of the droplet in (A) after quenching reveals that the nanoparticle assemblies are more disordered, but they still retain their linear shape, confirming their robust structure after cross-linking. Scale bars, 25 μm.

CONCLUSION

In summary, the elastic energy of liquid crystals can mitigate and shape the interfacial assembly of surface-active nanoparticles. We show that cholesterics can serve as templates for nanoparticles to be molded into arrangements with tunable length scales down to hundreds of nanometers by modifying both the surfactant and the chiral dopant concentrations. Furthermore, adjusting the nanoparticle to be more hydrophobic reveals the dynamics of assemblies toward interfacial coverage to be reminiscent of nucleation and growth. Last, we establish that these arrangements are easily cross-linkable from altering the surrounding aqueous phase. The properties of assemblies can be further customized because nanoparticle surface modification is accomplished via simple, in situ electrostatic adsorption. Many materials can have equally facile surface modifications, and silica nanoparticles with alternative compositions at their core can also be synthesized. Moreover, for nanoparticles to locate only in regions of favorable anchoring, the particles are required to strike a balance in their hydrophobicity, to be both interfacially active, yet mutually repulsive. A system with sensitivity to this balance is uncharted territory in the study of nanoparticle-decorated emulsions. Future investigations can use how nanoparticles either conform to or resist the liquid crystal surface pattern to better understand inter-nanoparticle interactions. This work establishes liquid crystal–patterned, nanoparticle-decorated emulsions as a system that combines interfacial phenomena with elasticity to not only design structures but also possibly investigate nanoparticle behaviors at interfaces.

MATERIALS AND METHODS

Materials

Amine-functionalized, fluorescent dye–coupled, 200-nm silica nanoparticles were synthesized by following the procedure described below. The materials for this procedure, fluorescein isothiocyanate isomer I (FITC), (3-aminopropyl)trimethoxysilane (APTMS; 97%), (3-aminopropyl) triethoxysilane (APTES; 99%), an aqueous solution of sodium hydroxide (NaOH; 0.1 M), and tetraethylorthosilicate (TEOS; 98%), were purchased from Sigma-Aldrich. Ammonium hydroxide (NH_4OH; 30%) was purchased from Fisher Scientific. Bare, fluorescent-core, 30-nm silica nanoparticles were purchased from Creative Diagnostics and were suspended in an aqueous solution at pH 6. SA_nS and C_8TAB were also obtained from Sigma-Aldrich. The lipids 1,2-dilauroyl-*sn*-glycero-3-phosphocholine (DLPC), labeled with 1 mole percent (mol %) Texas Red 1,2-dihexadecanoyl-*sn*-glycero-3-phosphoethanolamine, triethylammonium salt (TR-DHPE), were obtained from Avanti Polar Lipids. HCl, used for adjusting solution pH, was also obtained from Fisher Scientific. For the cholesteric liquid crystal, we used 5CB (Kingston Chemicals Limited) doped with CB15 (EMD Performance Materials and Synthon

Chemicals) for a right-handed cholesteric pitch. Glass surfaces brought into contact with surfactant-functionalized nanoparticles were rinsed with 2 wt % poly(diallyldimethylammonium chloride) (PDADMAC) (MW = 200, 000 to 300, 000 g/mol; Sigma-Aldrich) in a solution of 0.5 M sodium chloride (NaCl; Fisher Scientific). This treats the glass to minimize emulsion droplets adhering to it.

Optical characterization

The main confocal microscopy system used in experiments was an Olympus IX73 microscope coupled with a Thorlabs confocal microscopy upgrade. A blue laser (488 nm) was used for fluorescent dye excitation. The fluorescent light was collected through a 25-μm pinhole and passed through optical filters, transparent for wavelengths from 505 to 550 nm for FITC-labeled nanoparticles on the detector. The software ThorImage 3.1 was used for image acquisition. Confocal *z* stacks were obtained by a motorized focus control, with *z*-stack step sizes of 1 μm. ImageJ was used for the 2D projections of the confocal *z* stacks. For lipid measurements, confocal micrographs were obtained using an upright Leica TCS SP5 microscope. DLPC labeled with 1 mol % TR-DHPE was used to determine the surfactant location on the cholesteric liquid crystal–water interface. A scanning laser wavelength of 543 nm was used to excite TR-DHPE.

Stripe growth image analysis

Confocal *z*-stack projections were thresholded and binarized in ImageJ. Manual adjustments to separate pixels from adjacent stripes were done when necessary. To measure the total stripe length, stripes were skeletonized (reduced to 1-pixel width), and the number of pixels was measured and converted to micrometers. To measure the length of individual stripes, the image width and height of the skeletonized images were quadrupled to increase the width of the stripes again. The ImageJ feature "Analyze Particles" was used to measure the area of each individual stripe, which was used to calculate the length.

Fluorescent lipid patterning on a thin cholesteric film

With DLPC (Avanti Polar Lipids), labeled with 1 mol % TR-DHPE, as the surfactant, the water phase is a tris-buffered saline solution (10 mM tris, Fisher Scientific; 0.1 M NaCl, adjusted to pH 8.9 with HCl, Fisher Scientific) with a dispersion of vesicles 50 nm in diameter, following the procedure of previous work (*14*). A similar procedure from this work was also used for creating a thin cholesteric film in a copper transmission electron microscope grid on a cover glass treated with octadecyltrimethoxysilane (Sigma-Aldrich).

Liquid crystal Pickering emulsion preparation

All glass surfaces in contact with the emulsions, from the vials to the slides to the transfer pipettes (Fisher Scientific), were all treated with PDADMAC before use, as described in the "Materials" section. Samples were always made with fresh surfactant stock solutions to minimize the effects of hydrolysis and of carbon dioxide absorption and were measured to have a pH range of 7 to 7.5. When titrating components into the solution, nanoparticles were diluted first, then the pH was adjusted by additions of either HCl or NaOH. This was vortexed before the surfactant was added. The nanoparticle solution was then bath sonicated for 30 min before the cholesteric liquid crystal was introduced. Approximately 10 μl of the liquid crystal was pipetted to 1 ml of the nanoparticle solution. Liquid crystal in water emulsions was then created by simple shaking. Samples were viewed under the confocal microscope in a covered, hydrated container to minimize evaporation.

Preparation of dye-coupled, 200-nm silica nanoparticles

This procedure was done following the steps outlined by Lee and Yang (*43*). Briefly, FITC (Sigma-Aldrich) molecules were covalently bonded with APTMS (Sigma-Aldrich). First, 0.0015 g of FITC was dissolved in 2 ml of ethanol and mixed with 0.237 ml of APTMS for 12 hours under stirring with a Teflon-coated magnetic stir bar. Meanwhile, silica nanoparticles with a diameter of 200 nm (dispersed in deionized water), purchased from General Engineering & Research (San Diego, CA), were redispersed in ethanol in a sonication bath for 1 hour. Then, 32.5 ml of an ethanol suspension containing 1 wt % silica particles was mixed with 2.755 ml of ammonia for 10 min. Then, 0.689 ml of 0.1 M NaOH aqueous solution was poured into the bath to activate the silanol groups on the particle surface.

To couple the dye to the particles, 208 μl of as-prepared, FITC-APTMS solution was added to the silica suspension. After 5 min of thorough mixing, 40 μl of TEOS (Sigma-Aldrich) was added dropwise, and the mixture was reacted for 22 hours under stirring. To remove unreacted dye molecules, the resultant dye-coupled particles were washed with ethanol three times by centrifuging and replacing the supernatant with fresh ethanol.

Amine functionalization of dye-coupled silica

The procedure was done following the steps outlined by Jang *et al.* (*44*). Briefly, for the functionalization of silica particles, 0.23 g of silica pellet (as prepared above) was redispersed in 40 ml of fresh ethanol in a sonication bath. Under stirring with a Teflon-coated magnetic bar, 4 ml of ammonia solution (0.727 M in ethanol) was added. APTES solution (170 μl; 0.011 M in ethanol) was then slowly added dropwise to the silica dispersion. After 15 hours, the resultant solution was washed with ethanol five times by centrifugation to remove the unreacted APTES molecules.

$LaCl_3$ cross-linking of silica nanoparticles within stripes

Nanoparticles were aligned within stripes on the surface of cholesteric droplets in a solution of water with 0.01 wt %, 30-nm nanoparticles, 5 mM C_8TAB, and 0.2 mM HCl (Fig. 2). Excess nanoparticles were removed by gently replacing the supernatant with a solution of water with only 5 mM C_8TAB and 0.2 mM HCl. This is repeated three times. The nanoparticles at the interface were then cross-linked within stripes by replacing the supernatant with an aqueous solution with 5 mM C_8TAB, 0.2 mM HCl, and 0.5 mM $LaCl_3$. After leaving the sample to sit for ~5 min, the rinsing procedure was performed again with a similar aqueous solution that excludes the $LaCl_3$.

SUPPLEMENTARY MATERIALS

Supplementary material for this article is available at http://advances.sciencemag.org/cgi/content/full/4/10/eaat8597/DC1

Movie S1. Video of Fig. 4A, constructed from confocal micrographs, depicting nanoparticles adsorbing onto cholesteric liquid crystal droplets in a solution with 0.01 wt % of 30-nm, bare silica particles, 10 mM C_8TAB, and 0.23 mM HCl.

Fig. S1. Behavior of amine-functionalized silica nanoparticles, modified by varying concentrations of SOS, on cholesteric liquid crystal droplets in water (pH 7).

Fig. S2. Behavior of 0.0025 wt % of 200-nm, amine-functionalized silica nanoparticles, modified by varying the tail length of SA_nS, on cholesteric liquid crystal droplets in water (pH 7).

Fig. S3. Zeta potential measurements of solutions of particles and surfactants used in experiments.

Fig. S4. Analysis of the growth of nanoparticle-filled stripes on a cholesteric liquid crystal droplet.
Fig. S5. Destroying cholesteric ordering with temperature.

REFERENCES AND NOTES

1. G. M. Whitesides, B. Grzybowski, Self-assembly at all scales. *Science* **295**, 2418–2421 (2002).
2. E. Lee, Y. Xia, R. C. Ferrier Jr., H.-N. Kim, M. A. Gharbi, K. J. Stebe, R. D. Kamien, R. J. Composto, S. Yang, Fine golden rings: Tunable surface plasmon resonance from assembled nanorods in topological defects of liquid crystals. *Adv. Mater.* **28**, 2731–2736 (2016).
3. S. K. Kumar, N. Jouault, B. Benicewicz, T. Neely, Nanocomposites with polymer grafted nanoparticles. *Macromolecules* **46**, 3199–3214 (2013).
4. J. J. Chiu, B. J. Kim, E. J. Kramer, D. J. Pine, Control of nanoparticle location in block copolymers. *J. Am. Chem. Soc.* **127**, 5036–5037 (2005).
5. D. Coursault, J. Grand, B. Zappone, H. Ayeb, G. Lévi, N. Félidj, E. Lacaze, Linear self-assembly of nanoparticles within liquid crystal defect arrays. *Adv. Mater.* **24**, 1461–1465 (2012).
6. J. S. Pendery, O. Merchiers, D. Coursault, J. Grand, H. Ayeb, R. Greget, B. Donnio, J.-L. Gallani, C. Rosenblatt, N. Félidj, Y. Borensztein, E. Lacaze, Gold nanoparticle self-assembly moderated by a cholesteric liquid crystal. *Soft Matter* **9**, 9366–9375 (2013).
7. M. Mitov, C. Portet, C. Bourgerette, E. Snoeck, M. Verelst, Long-range structuring of nanoparticles by mimicry of a cholesteric liquid crystal. *Nat. Mater.* **1**, 229–231 (2002).
8. H. Qi, T. Hegmann, Formation of periodic stripe patterns in nematic liquid crystals doped with functionalized gold nanoparticles. *J. Mater. Chem.* **16**, 4197–4205 (2006).
9. A. L. Rodarte, R. J. Pandolfi, S. Ghosh, L. S. Hirst, Quantum dot/liquid crystal composite materials: Self-assembly driven by liquid crystal phase transition templating. *J. Mater. Chem. C* **1**, 5527–5532 (2013).
10. R. Bitar, G. Agez, M. Mitov, Cholesteric liquid crystal self-organization of gold nanoparticles. *Soft Matter* **7**, 8198–8206 (2011).
11. L. Tran, M. O. Lavrentovich, G. Durey, A. Darmon, M. F. Haase, N. Li, D. Lee, K. J. Stebe, R. D. Kamien, T. Lopez-Leon, Change in stripes for cholesteric shells via anchoring in moderation. *Phys. Rev. X* **7**, 041029 (2017).
12. R. Costi, A. E. Saunders, U. Banin, Colloidal hybrid nanostructures: A new type of functional materials. *Angew. Chem. Int. Ed.* **49**, 4878–4897 (2010).
13. A. Darmon, M. Benzaquen, D. Seč, S. Čopar, O. Dauchot, T. Lopez-Leon, Waltzing route toward double-helix formation in cholesteric shells. *Proc. Natl. Acad. Sci. U.S.A.* **113**, 9469–9474 (2016).
14. J. M. Brake, M. K. Daschner, Y.-Y. Luk, N. L. Abbott, Biomolecular interactions at phospholipid-decorated surfaces of liquid crystals. *Science* **302**, 2094–2097 (2003).
15. F. Mondiot, X. Wang, J. J. de Pablo, N. L. Abbott, Liquid crystal-based emulsions for synthesis of spherical and non-spherical particles with chemical patches. *J. Am. Chem. Soc.* **135**, 9972–9975 (2013).
16. J. Noh, B. Henx, J. P. F. Lagerwall, Taming liquid crystal self-assembly: The multifaceted response of nematic and smectic shells to polymerization. *Adv. Mater.* **28**, 10170–10174 (2016).
17. R. Meister, H. Dumoulin, M.-A. Hallé, P. Pieranski, The anchoring of a cholesteric liquid crystal at the free surface. *J. Phys. II* **6**, 827–844 (1996).
18. R. Meister, M.-A. Hallé, H. Dumoulin, P. Pieranski, Structure of the cholesteric focal conic domains at the free surface. *Phys. Rev. E* **54**, 3771–3782 (1996).
19. Y. Bouligand, F. Livolant, The organization of cholesteric spherulites. *J. Phys. France* **45**, 1899–1923 (1984).
20. J. A. Moreno-Razo, E. J. Sambriski, N. L. Abbott, J. P. Hernández-Ortiz, J. J. de Pablo, Liquid-crystal-mediated self-assembly at nanodroplet interfaces. *Nature* **485**, 86–89 (2012).
21. M. Rahimi, T. F. Roberts, J. C. Armas-Pérez, X. Wang, E. Bukusoglu, N. L. Abbott, J. J. de Pablo, Nanoparticle self-assembly at the interface of liquid crystal droplets. *Proc. Natl. Acad. Sci. U.S.A.* **112**, 5297–5302 (2015).
22. I. I. Smalyukh, S. Chernyshuk, B. I. Lev, A. B. Nych, U. Ognysta, V. G. Nazarenko, O. D. Lavrentovich, Ordered droplet structures at the liquid crystal surface and elastic-capillary colloidal interactions. *Phys. Rev. Lett.* **93**, 117801 (2004).
23. I. B. Liu, M. A. Gharbi, V. L. Ngo, R. D. Kamien, S. Yang, K. J. Stebe, Elastocapillary interactions on nematic films. *Proc. Natl. Acad. Sci. U.S.A.* **112**, 6336–6340 (2015).
24. M. A. Gharbi, M. Nobili, M. In, G. Prévot, P. Galatola, J.-B. Fournier, C. Blanc, Behavior of colloidal particles at a nematic liquid crystal interface. *Soft Matter* **7**, 1467–1471 (2011).
25. J. S. Lintuvuori, A. C. Pawsey, K. Stratford, M. E. Cates, P. S. Clegg, D. Marenduzzo, Colloidal templating at a cholesteric-oil interface: Assembly guided by an array of disclination lines. *Phys. Rev. Lett.* **110**, 187801 (2013).
26. J. M. Brake, N. L. Abbott, An experimental system for imaging the reversible adsorption of amphiphiles at aqueous-liquid crystal interfaces. *Langmuir* **18**, 6101–6109 (2002).
27. U. T. Gonzenbach, A. R. Studart, E. Tervoort, L. J. Gauckler, Stabilization of foams with inorganic colloidal particles. *Langmuir* **22**, 10983–10988 (2006).
28. B. P. Binks, J. A. Rodrigues, Enhanced stabilization of emulsions due to surfactant-induced nanoparticle flocculation. *Langmuir* **23**, 7436–7439 (2007).
29. M. F. Haase, K. J. Stebe, D. Lee, Continuous fabrication of hierarchical and asymmetric bijel microparticles, fibers, and membranes by solvent transfer-induced phase separation (STRIPS). *Adv. Mater.* **27**, 7065–7071 (2015).
30. R. J. Hunter, *Zeta Potential in Colloid Science: Principles and Applications* (Academic Press, 2013), vol. 2.
31. I. Akartuna, A. R. Studart, E. Tervoort, U. T. Gonzenbach, L. J. Gauckler, Stabilization of oil-in-water emulsions by colloidal particles modified with short amphiphiles. *Langmuir* **24**, 7161–7168 (2008).
32. M. F. Haase, D. Grigoriev, H. Moehwald, B. Tiersch, D. G. Shchukin, Encapsulation of amphoteric substances in a pH-sensitive Pickering emulsion. *J. Phys. Chem. C* **114**, 17304–17310 (2010).
33. V. Garbin, J. C. Crocker, K. J. Stebe, Forced desorption of nanoparticles from an oil–water interface. *Langmuir* **28**, 1663–1667 (2012).
34. S. M. Kirby, S. L. Anna, L. M. Walker, Effect of surfactant tail length and ionic strength on the interfacial properties of nanoparticle-surfactant complexes. *Soft Matter* **14**, 112–123 (2018).
35. Z.-G. Cui, L.-L. Yang, Y.-Z. Cui, B. P. Binks, Effects of surfactant structure on the phase inversion of emulsions stabilized by mixtures of silica nanoparticles and cationic surfactant. *Langmuir* **26**, 4717–4724 (2010).
36. R. Cano, Interprétation des discontinuités de grandjean. *Bull. Soc. Fr. Mineral. Cristallogr.* **91**, 20 (1968).
37. F. Grandjean, Sur l'existence de plans différenciés équidistants normaux à l'axe optique dans les liquides anisotropes (cristaux liquides). *C. R. Seances Acad. Sci. Paris* **172**, 71 (1921).
38. P. L. Krapivsky, S. Redner, E. Ben-Naim, *A Kinetic View of Statistical Physics* (Cambridge Univ. Press, 2010).
39. M. E. Leunissen, A. van Blaaderen, A. D. Hollingsworth, M. T. Sullivan, P. M. Chaikin, Electrostatics at the oil–water interface, stability, and order in emulsions and colloids. *Proc. Natl. Acad. Sci. U.S.A.* **104**, 2585–2590 (2007).
40. A. T. Skjeltorp, Visualization and characterization of colloidal growth from ramified to faceted structures. *Phys. Rev. Lett.* **58**, 1444–1447 (1987).
41. G. Meng, J. Paulose, D. R. Nelson, V. N. Manoharan, Elastic instability of a crystal growing on a curved surface. *Science* **343**, 634–637 (2014).
42. W. J. Frith, R. Pichot, M. Kirkland, B. Wolf, Formation, stability, and rheology of particle stabilized emulsions: Influence of multivalent cations. *Ind. Eng. Chem. Res.* **47**, 6434–6444 (2008).
43. S. Y. Lee, S. Yang, Compartment fabrication of magneto-responsive Janus microrod particles. *Chem. Commun.* **51**, 1639–1642 (2015).
44. S. G. Jang, S.-H. Kim, S. Y. Lee, W. C. Jeong, S.-M. Yang, Facile synthesis of core-shell and Janus particles via 2-D dendritic growth of gold film. *J. Colloid. Interface. Sci.* **350**, 387–395 (2010).

Acknowledgments: We thank A. Dang, G. Durey, S. Hann, E. Horsley, E. Lacaze, D. Lee, T. Lopez-Leon, and Y. Xia for materials and helpful discussions. We thank S. S. Margulies and D. F. Meaney for access to confocal microscopy and G. Gray Lawrence for help with confocal measurements. **Funding:** This work was supported by NSF Materials Research Science and Engineering Centers (MRSEC) grant DMR-1720530. L.T. acknowledges support from an American Fellowship grant from the American Association of University Women and from the Simons Society of Fellows of the Simons Foundation. M.F.H. was supported by NSF CAREER award CBET-1751479. R.D.K. was partially supported by a Simons Investigator grant from the Simons Foundation. **Author contributions:** L.T. and M.F.H. designed the research. L.T., H.-N.K., N.L., and M.F.H. performed the research. L.T., H.-N.K., N.L., S.Y., K.J.S., R.D.K., and M.F.H. analyzed the data and wrote the paper. **Competing interests:** The authors declare that they have no competing interests. **Data and materials availability:** All data needed to evaluate the conclusions in the paper are presented in the paper and/or the Supplementary Materials. Additional data related to this paper may be requested from the authors.

Submitted 11 April 2018
Accepted 4 September 2018
Published 12 October 2018
10.1126/sciadv.aat8597

Citation: L. Tran, H.-N. Kim, N. Li, S. Yang, K. J. Stebe, R. D. Kamien, M. F. Haase, Shaping nanoparticle fingerprints at the interface of cholesteric droplets. *Sci. Adv.* **4**, eaat8597 (2018).

ScienceAdvances

Shaping nanoparticle fingerprints at the interface of cholesteric droplets

Lisa Tran, Hye-Na Kim, Ningwei Li, Shu Yang, Kathleen J. Stebe, Randall D. Kamien and Martin F. Haase

Sci Adv **4** (10), eaat8597.
DOI: 10.1126/sciadv.aat8597